

A toolkit for multi-scale mapping of the solar energy-generation potential of buildings in urban environments under uncertainty

G. Peronato^{a,*}, P. Rastogi^{b,1}, E. Rey^c, M. Andersen^a

^a*Ecole polytechnique fédérale de Lausanne (EPFL),
Laboratory of Integrated Performance in Design (LIPID)*

^b*University of Strathclyde,
Dept. of Mechanical and Aerospace Engineering,
Energy Systems Research Unit (ESRU)*

^c*Ecole polytechnique fédérale de Lausanne (EPFL),
Laboratory of Architecture and Sustainable Technologies (LAST)*

Abstract

Many municipalities and public authorities have supported the creation of solar cadastres to map the solar energy-generation potential of existing buildings. Despite advancements in modelling solar potential, most of these tools provide simple evaluations based on benchmarks, neglecting the effect of uncertain environmental conditions and that of the spatial aggregation of multiple buildings. We argue that including such information in the evaluation process can lead to more robust planning decisions and a fairer allocation of public subsidies.

To this end, this paper presents a novel method to incorporate uncertainty in the evaluation of the solar electricity generation potential of existing buildings using a multi-scale approach. It also presents a technique to visualise the results through their integration in a 3D-mapping environment and the use of false-colour overlays at different scales.

Using multiple simulation scenarios, the method is able to provide information about confidence intervals of summary statistics of production due to variation in two typical uncertain factors: vegetation and weather. The uncertainty in production introduced by these factors is taken into account through pairwise comparisons of nominal values of indicators, calculating a comprehensive ranking of the energy potential of different spatial locations and a corresponding solar score. The analysis is run at different scales, using space- and time-aggregated results, to provide results relevant to decision-makers.

Keywords: urban solar potential, spatial decision-support systems, 3D city model

*Corresponding author

Email address: giuseppe.peronato@epfl.ch or gperonato@gmail.com (G. Peronato)

¹Swiss National Science Foundation visiting scientist

1. Introduction

The installation of photovoltaic (PV) systems in urban contexts is increasingly viable from both practical and commercial viewpoints. The simplest evaluation of the economic or environmental viability of a project is to examine the lifetime costs of installation, maintenance, and disposal versus the value of electricity produced. Given the multiplicity of potential sites in a city or on an estate, planners and large land owners are often tasked with prioritising the allocation of resources to sites based on their technical and commercial viability.

This paper presents approaches to making these decisions using simulations under uncertain environmental conditions. We have developed a method for comparing the potential of different urban sites to generate energy using photovoltaic systems. The method, embedded in a 3D mapping tool, provides an uncertainty-aware ranking of candidate locations for a multi-stage and multi-scale urban planning processes.

1.1. *The problem*

Simulating the behaviour of a physical system involves the consideration of fixed and random inputs, both of which might be known only with partial confidence. For any weather-dependent system, like buildings or solar power installations, the future weather is an uncertain boundary condition. The evaluation of solar installations in urban areas must also take into account the presence of obstructions, which are chiefly caused by urban vegetation and surrounding buildings or infrastructure. However, in the case of vegetation, the specific transparency and seasonal change of each tree are difficult to predict and are, therefore, also a source of uncertainty.

In order to provide robust planning decisions, we consider these uncertain factors in evaluating the suitability of different urban locations (hereinafter, plots) for photovoltaic installations. In a deterministic study, i.e., one in which all inputs are fixed to some nominal values, comparing and ranking different plots is straightforward. One could, for example, sort the plots by annual sum of production. However, the introduction of uncertain inputs complicates the comparison of options because different plots and systems respond differently to changes in those inputs. This creates an issue for planners and decision-makers, who have to make a definite decision but who cannot get a definite answer from a simulation study.

1.2. *State of the art*

The increasing availability of detailed geodata sets and improvements in computational models have made the assessment and visualization of solar potential at the urban scale a popular tool for planners. An extensive literature review can be found in Freitas et al. (2015). Recent implementations have extended the analysis to vertical surfaces (Catita et al., 2014; Bremer et al., 2016; Brito et al., 2017), but the evaluation is still commonly done in 2(.5)D, i.e., targeting only roof surfaces. These evaluations do not consider the varying effects of vegetation and weather on the evaluated surfaces.

Current methods are usually limited to the assessment of an installation itself, neglecting the subsequent use of the results of the assessment in the decision-making process. In fact,

it is in this phase that uncertainty in the outputs could play an important role and should, therefore, be considered by risk-aware and risk-averse decision-makers. In this section, we review decision-making methods for assessing solar potential and their limits. We also investigate other methods that can be applied to this scope.

1.2.1. Decision-making for solar potential assessment

Solar cadastres (or solar maps) are tools to provide decision-makers with information about the suitability of a given surface for the installation of solar power systems (photovoltaic or thermal). They are usually conceived as web-based mapping tools in which the solar potential is displayed as false-colours overlays on 2D maps or ortho-photos of an urban area. Dean et al. (2009) and Kanters et al. (2014) provide an extensive review of solar cadastres in Europe and United States. Although methods considering weather risk have been integrated in PV-array performance evaluation software (Dobos et al., 2012), to the best of our knowledge, evaluations included in solar cadastres are conducted using weather data from typical meteorological years (TMY), whose limitations have been described by Vignola et al. (2012).

As shown by Kanters et al. (2014), the suitability assessment of solar cadastres is generally based on minimum irradiation thresholds. In some cases, the choice of these thresholds is justified by financial assessments to guarantee the payback time of the installation (Nault et al., 2015; Jakubiec and Reinhart, 2013; Berlin et al., 2013). Surfaces are often classified with different levels of suitability depending on their solar irradiation, such as ‘reasonable’, ‘good’, ‘very good’ (Kanters et al., 2014).

Previous work (Nault et al., 2015; Peronato et al., 2015, 2016a, 2017a) has highlighted that error, risk, and uncertainty vary depending on the selected threshold. However, solar cadastres generally have a deterministic approach, which neglects the uncertainty of the result and the concomitant risk in the decision. Thresholds are also sensitive to the geometric regularity of the arrangement of solar modules (Peronato et al., 2015), an aspect that is also neglected in solar assessment tools.

In addition to thresholds, another method to provide information about solar potential is to attribute to each building a solar score. The solar score is usually calculated by reference to a best-case installation, as in the Mapdwell solar maps (Berlin et al., 2013), or by normalising the data to the best and worst values in a given location, as in the SunNumber website (Miller and Herrmann, 2016). This method facilitates comparisons between locations with non-homogeneous climate conditions as the score is relative to the specific conditions, allowing cross-country comparisons. However, the score still disregards other factors of uncertainty in the calculation which affect each building differently, such as vegetation modelling.

Solar cadastres focus on the potential of individual buildings, and in some cases differentiate the potential among the surfaces constituting the building envelope, while neglecting the aggregated potential of urban blocks or entire urban areas. They are targeted towards building owners, and often have an educational goal (Dean et al., 2009). They are sometimes used as back-end planning tools by municipalities, though mostly limited to the evaluation of their own real estate properties (Kanters et al., 2014).

Energy-planning tools focus more explicitly on a wider range of stakeholders, particularly utility companies and municipalities. In this sense, Ouhajjou et al. (2014, 2015, 2016) proposed an ontology-based urban energy planning providing a classification of the PV-suitability of buildings from each stakeholder's perspective. However, this method then focuses on negotiation and consensus between the different stakeholders rather than the robustness of the single decision.

1.2.2. Ranking methods

In spatial planning, multi-criteria methods are used to define priorities among different locations, i.e., ranking options by priority of intervention. Recent sample applications include the definition of best locations for treated waste-water in-stream use (Kim et al., 2013). Ranking is a typical problem in multi-criteria decision-making, along with choice and sorting (Schärlig, 1985, Ch. 4c). The distinction between choice and ranking is not always clear, as ranking procedures can be adopted in decision problems that are more choice-like to give more options to the decision-maker (Schärlig, 1996, Ch. 10). Sorting can also be applied to ranked solutions by subsequent attribution to different categories. In this sense, ranking provides the simplest way to approach a decision problem, while allowing the decision-makers to introduce further choice- and/or sorting-based decisions.

Pairwise comparisons are often used in decision problems, as they are an effective method to subdivide a complex decision problem into binary preference questions. This is especially necessary when the criteria by which the alternatives are ranked or chosen are subjective and hence prone to inconsistency. The Analytical Hierarchical Process (AHP) (Saaty, 1980) and the outranking methods of the Electre (Roy and Vincke, 1984) and Prométhée (Brans, 1982) families make use of pairwise comparisons for decision problems involving both tangible and intangible (e.g., qualitative) criteria. Pairwise comparisons are also used when a preference model can only be applied to pairs of items at a time. This is the case, for example, in sport tournaments: only two teams can play each other at once, so a pool of n teams will require $(n^2 - n)/2$ matches (or $n^2 - n$ matches if home- and away-games are considered) to obtain a final ranking of the teams.

Condorcet methods are some of the most popular pairwise ranking methods, with applications in both sport tournaments and elections. These methods calculate the score of each player/candidate as the number of victories by pairwise comparisons. The players are ranked based on the final score of each player, and ranking may include ties. An extension of the Condorcet method, the Copeland method (Pomerol and Barba-Romero, 2012, p. 122), also counts the defeats. It can be seen as a special case of the Borda count method (Shah and Wainwright, 2015), another popular method used in both elections and sports, which generally requires multiple matches between the same pair of opponents (or a ballot asking voters to rank the different candidates) to establish the final ranking. The Copeland method provides simple, robust and optimal ranking from pairwise comparisons (Shah and Wainwright, 2015). It is often criticised because it counts only the quantity of victories and defeats and ignores their magnitude. This limitation can be overcome by accepting fuzzy outcomes and introducing fractional scores, instead of the conventional boolean/crisp comparisons between alternatives, e.g., Naderi et al. (2012).

1.2.3. Dealing with uncertainty

Most methods for solving spatial-decision problems assume that complete information is available, so that decision-makers know the outcome of their choice precisely. However, in real-world applications, this is often not the case. In spatial decision problems, uncertainty can be related to errors in position or attributes (Malczewski and Rinner, 2015, 7.2.2.2), or the preferences of decision-makers (Malczewski, 1999, 8.1.2). In this work, we will focus on attribute errors and will only consider decisions based on a single criterion.

Methods to account for uncertainty can be categorised as either direct methods, which include uncertainty directly in the preference model (e.g., by the use of probabilistic and fuzzy decision types), or indirect methods, which quantify the uncertainty by sampling different inputs. Typical indirect approaches to quantifying uncertainty are sensitivity and error propagation analyses. The main difference is that while the latter work by propagating perturbations or variations of the inputs through the model, the former incorporate the error/uncertainty associated with each parameter in the model itself (Malczewski, 1999, 8.2). Indirect methods can be used to test the robustness of a decision to the variation of some parameters, while direct methods are aimed at making the preference model robust to such variations.

As shown by Malczewski (1999, 8.2), an alternative A_i is preferred to A_k if the lowest value of the i 'th criterion outcome ($V_i - \sigma_{V_i}$) is greater than the highest value of the k 'th outcome ($V_k + \sigma_{V_k}$), i.e.,

$$A_i > A_k \quad \text{if, and only if,} \quad (V_i - \sigma_{V_i}) \geq (V_k + \sigma_{V_k}). \quad (1)$$

By this criterion, an alternative may not be selected over another when there is an overlap of the range of the chosen outputs, as shown in Fig. 1. We call this *risk-averse* decision-making, and discuss it further in Section 2.3.1.

1.3. Our proposal

We have seen that ranking methods are commonly used in spatial planning. We argue that such methods can also be applied to the assessment of solar potential to define priority intervention areas, while integrating the uncertainty related to the outputs.

When evaluating alternative outcomes under uncertainty, we can apply the preference model proposed by Malczewski (1999) (Eq. 1), which returns three preference situations. If we consider the incomparability situation as a tie score in a match, we can then use pairwise comparisons to provide a final ranking like in a sport tournament, using the Copeland method. Moreover, using a fuzzy evaluation can help consider not only the number of victories/defeats but also their magnitude.

Therefore, this work proposes a novel method of assessing solar energy potential based on the uncertainty-aware ranking of different urban locations. The method is multi-scale and multi-user, fitting well with the many stages and scales of the urban planning processes, while providing an effective visualization like existing web-based solar cadastres.

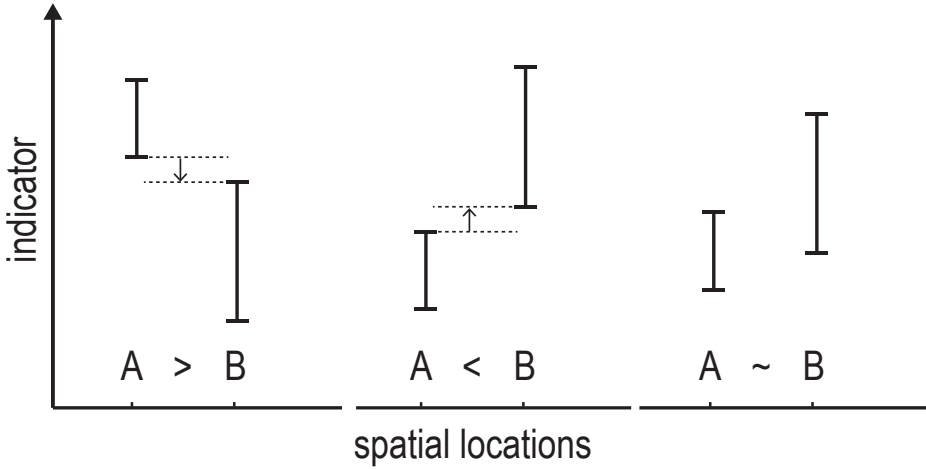


Figure 1: Risk-averse preference model, adapted from Malczewski (1999). In the left-most case, A is *always* better than B, while the opposite is true in the central case. A risk-averse decision-maker would be unable to make a decision in the right-most case since there is overlap.

1.4. Structure of the paper

In Section 2, we present the general characteristics of the proposed method. Subsequently, in Section 3, we describe the implementation of the method in a simulation-based workflow, describing the tools and the data used for the case-study analysis. The results of the case-study are presented in Section 4, where both case-specific and general findings are discussed. In section 5, we discuss limitations and future work, and in Section 6 we summarise the main findings of this study.

2. Method

As we have discussed in the introduction, there is no ‘standard’ method to compare two candidate locations for installing solar systems. Instead, the choice of outputs and statistics to be compared is governed by the priorities of the project and the risk attitude of the decision maker.

In this paper, we show the application of the method using one indicator of solar potential: the **normalised gross electric energy production**, i.e., the sum of DC power at maximum power point produced every hour (gross electric energy production), assuming that the production is constant during that hour [Wh], normalised by the peak power installed [Wp]. We consider here DC electricity production as a proxy for AC electricity production, which is the relevant quantity assessing the performance of the solar system. Other indicators will be discussed in Section 5.

2.1. Spatial division

This work considers a typical problem of spatial decision making: the evaluation of multiple locations to find the most suitable one(s) for some given goals and constraints. The simulation of solar radiation and PV production is conducted at the panel level, and these quantities are aggregated at different spatial divisions to be meaningful for different decision makers. For example, an owner of a housing estate may be interested in finding the optimal roof location from a collection of buildings in a relatively small area. Spatial divisions could be based on ground conditions such as planning laws and decisions, constructions, or abstractions such as Cartesian coordinates. We use the generic word ‘plot’ in subsequent discussions, with the implication that it could mean any spatial division of interest. From the non-exhaustive list that follows, we used Cartesian tiles in this paper:

Surfaces – as defined in the 3D cadastre, excluding surfaces of architectural details such as dormers and constructions not classified as buildings.

Buildings – as defined in the 3D cadastre.

Planning zones – homogeneous urban areas, as defined in the local planning tools.

Tiles – a Cartesian subdivision of the space into squares of equal areas.

2.2. Modelling scenarios

The method relies on simulations using a detailed geometric 3D-model (see Section 3.1.1), combined with a preference model. The preference model is based on uncertain inputs, i.e., inputs with aleatory and epistemic uncertainties. The former arises from not knowing the apparently random environmental conditions, and the latter from incomplete knowledge about the physical system itself (panels, installation, etc.). To obtain ranges of outputs, two types of simulations are used, one using nominal extreme inputs and another using random inputs.

Nominal inputs correspond to single ‘extreme’ scenarios. These are ‘artificial’ in the sense that they represent boundaries that are unlikely to be reached in a real scenario. Therefore, they provide conservative upper and lower bounds to the simulation outputs. The random inputs were generated by an algorithm applying a uniform distribution from two single scenarios (vegetation) described in Figure 2. In the absence of better information, we chose the uniform distribution. In future work, we will collect data to examine if other distributions could better describe the random inputs.

2.2.1. Vegetation

The vegetation 3D shape is reconstructed from LiDAR (Light Detection and Ranging) point-clouds obtained through Automated Laser scanning (ALS), using an approach adapted from Peronato et al. (2016b) that will be further explained in Section 3.1.1. The seasonal variation of the tree shape and its degree of transparency cannot be directly sensed from these data. In particular, in most situations it is not possible to establish whether a tree is deciduous or evergreen, unless multiple ALS are conducted in different seasons. Studies

retrieving to sense the tree species are usually conducted on limited species as typically found in forests (e.g. Korpela et al. (2010)), while in urban environments in temperate climates we can expect a very large number of species in public and private gardens. To obtain bounds on the influence of vegetation on production, we opted for two extreme scenarios which together cover the entire spectrum of possible vegetation conditions under different seasons:

Opaque trees – in which the vegetation is exclusively composed of evergreen trees.

No trees – in which the vegetation is without leaves all year-round, like deciduous trees in winter time.

Two approaches are then proposed: ranking using summary statistics based either on these two extreme scenarios or on multiple random vegetation input derived from these scenarios. The random vegetation input is composed by sampling each of these scenarios with equal probability at each time step using the algorithm described in Figure 2. The proportion of sensors blocked or not blocked by vegetation (obstructed vs unobstructed) is determined by taking an evenly-spaced sample from a standard uniform distribution, i.e., $P(op) \sim \mathcal{U}(0, 1)$ and $P(nt) = 1 - P(op)$ ($op \rightarrow \text{opaque}$, $nt \rightarrow \text{notrees}$). Then two ‘masks’ are prepared, one each for the *notrees* and *opaque* simulations. These masks are binary arrays, where a 1 corresponds to the shading condition for that panel/sensor being ‘on’ while a 0 corresponds to ‘off’. When these masks are applied to each simulation, and the two ‘masked’ simulations results added, the proportions of obstructed and unobstructed sensors in the resultant ‘synthetic simulation’ corresponds to $P(op)$ and $P(nt)$.

2.2.2. Weather/Climate

The weather input is based on a collection of measured/recorded time series from Neuchâtel, Switzerland, as described in Section 3.1.1. We need several years of measured data to extract both ‘typical’ and ‘extreme’ weather scenarios. The concept of a ‘typical year’ is described in previous studies by Wilcox and Marion (2008) and Cebecauer and Suri (2015), though in the case study for this paper we used the typical year produced with the software Meteonorm using datasets from the years 2000-2010 (Remund et al., 2012).

The ‘extreme’ weather scenario are composite years. Say we wish to create the q -th quantile composite year, where $q < 0.5$. Concatenating the q -th quantile months could result in a year whose annual cumulative radiation is much lower than the q -th quantile year selected based on annual cumulative radiation. So we switch out a random subset of months from the artificially-low composite year with one of up to n nearest neighbours of the q -th quantile month. This random switching is done until the resulting composite year has at least the same annual cumulative irradiation as the q -th quantile year selected based on annual cumulative radiation (within some tolerance, e.g., 10%). The procedure is the same for $q \geq 0.5$, except we search for a year that has at most the same annual sum.

This method is conceptually similar to Px years (Cebecauer and Suri, 2015) (where $x = 1 - q$), which produces years with a probability of exceedance x . That is, the probability of annual cumulative irradiation exceeding the Px value is $(100*x)\%$. Our procedure ignores

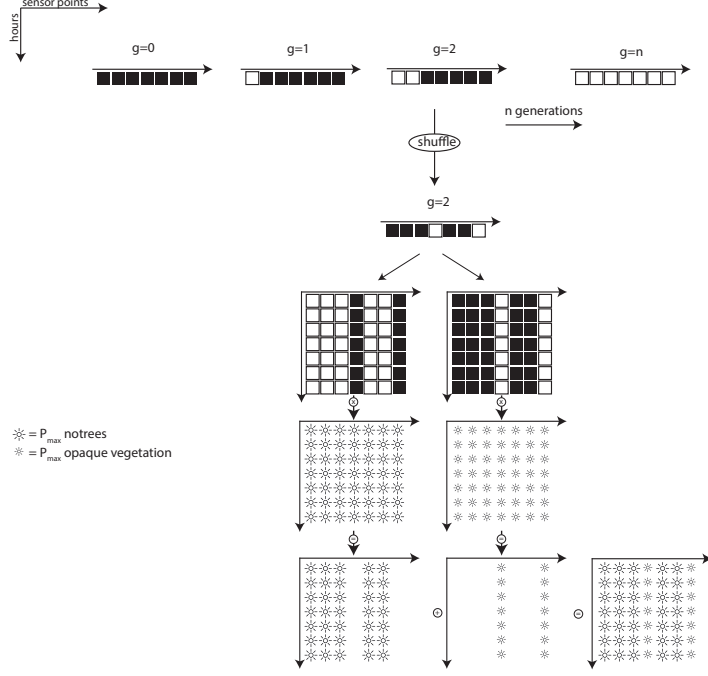


Figure 2: Sampling algorithm used to create the random vegetation scenarios from a standard uniform distribution of ‘notrees’ and ‘opaque’ scenarios.

the years that the months come from since the objective is to create artificial ‘bounds’ on the production. In this work, we use the label ‘low rad’ for composite years with $q = 10$ and ‘high rad’ for $q = 90$. We use the ‘extreme’ scenarios only to discard locations that might not achieve the selected threshold in non-favourable conditions. The actual indicators are calculated on the basis of ‘typical’ weather files.

2.3. Ranking from risk-averse comparisons

This method is meant to systematise decision-making about how to select one spatial location over another under uncertainty. We demonstrate an approach which is based on the comparison of summary statistics accounting for their confidence intervals. Based on the outcome of this preference model, we show an aggregation of its outcome into a ranking.

2.3.1. Preference model

This method is appropriate for epistemic sources of uncertainty such as vegetation. Remote-sensing data cannot properly characterise the transmission factor of the vegetation canopy and its seasonal variations. Therefore, we expect that the actual transparency level at any given time of year is somewhere between a fully-opaque tree canopy and a fully-transparent one. The extremes correspond to unrealistic boundary (environmental) conditions, but nevertheless have some advantages: they can be modelled easily and allow risk-averse decision-making.

To avoid risk completely, we should make the choice between two locations based on opposite extreme scenarios, as we cannot conclusively exclude the scenario that these two locations have opposite vegetation characteristics. That is, one zone has sparse, deciduous vegetation and the other has dense, evergreen vegetation. This leaves us with three possible outcomes of a comparison:

- if $\max(A) < \min(B)$ then $A < B$,
- if $\min(A) > \max(B)$ then $A > B$,
- else $A \sim B$,

where $\max(\cdot)$ corresponds to the ‘no trees’ scenario and $\min(\cdot)$ to the ‘opaque trees’ scenario. This model is represented in Figure 1.

We used the Copeland method, where each plot is compared to every other to determine winners and losers in a comprehensive pairwise match-up. Each comparison is carried out using ranges of outputs from a small set of annual simulations using extreme input conditions, which is a crude estimate of the range of annual sum of energy production values. The results of each match-up can be stored as all-or-none scores, i.e., +1 for a win, 0 for a tie, and -1 for a loss; or scaled scores, where each difference between two plots is stored as a fraction of the largest difference in a given group, e.g., 0.7 for a ‘large win’ or 0.25 for a ‘small win’. Each of these scoring systems may be thought of as representing different attitudes to risk: the all-or-none system is more risk-averse since inconsistent performers are less likely to stand out over a large number of match-ups. However, using the all-or-none principle implies the same risks as a first-past-the-post electoral system, i.e., the plot that has the highest number of wins is first, regardless of the number of wins as a proportion of the total match-ups or magnitude of these wins.

2.3.2. Ranking aggregation

There are three main methods to aggregate results from comparisons into a ranking: permutation-based, matrix factorisation, and score-based probabilistic methods (Liang and de Alfaro, 2017). Permutation methods are computationally expensive, while matrix factorisation and score-based methods provide an efficient way to obtain a ranking from pairwise comparisons (Feizizadeh et al., 2014).

We used a score-based method, as it provides decision-makers with an intuitive and easy system to compute rankings from multiple pairwise comparisons. Specifically, we applied Copeland’s method (Pomerol and Barba-Romero, 2012, p. 122), which tracks the number of victories or defeats from each pairwise comparison. In pairwise comparisons with expert answers, the decision matrix might be incoherent, since human experts may show inconsistency over time. As the outcomes in our method are derived from objective comparisons of the bootstrapped summary statistics of time series, the decision matrix is perfectly coherent. When the production from two plots is compared, the conditions under which each is tested are comparable.

These comparisons are symmetric, i.e. if $x > y$, then $y < x$. In this sense, the score calculated when comparing location x to y (± 1) has to be the additive inverse of the score calculated when comparing location y to x (∓ 1). Whenever a comparison yields no winner, because the variation in a summary statistic due to uncertain boundary conditions is larger than the difference between the two locations, the assigned score is 0.

As we discussed in the preference model above, for some risk attitudes, identifying the winner of each comparison is not enough to identify the best candidate. It is also necessary to quantify how much better (or worse) a location is compared to its opposing ones. To enable this comparison, we integrated a fuzzy logic system for both our preference models. This system is based on calculating *fractional wins*, i.e., the difference between two choices divided by a normalisation factor. The normalisation factor *norm* is

$$\text{norm} = |\max(\min(E_A - E_B)) - (\min(\max(E_A - E_B)))|,$$

i.e., the difference between the highest production using the min-radiation scenario (e.g., opaque vegetation) and the lowest production using the max-radiation scenario (e.g., no vegetation). This method results in a normalisation factor *norm* which is applied to the assigned *score*, so that the highest score ± 1 is only assigned to the victory/defeat with the largest margin. The preference model may then be summed as:

- if $\max(A) < \min(B)$ then $\text{score} = (\max(A) - \min(B))/\text{norm}$
- if $\min(A) > \max(B)$ then $\text{score} = (\min(A) - \max(B))/\text{norm}$
- else $\text{score} = 0$

2.4. Ranking with low-yield avoidance

The challenge of any climate-based simulation is to understand micro-climatic conditions, i.e., the local conditions experienced by a solar panel, while only having data about the conditions at the regional or global scale, i.e., smooth meso-scale data. In our analysis, we ignore the spatial variation of wind and temperature at the microclimatic scale. That is, we assume that the effect of the urban microclimate on temperature and wind speed is experienced uniformly by each plot/tile. We model the changes in solar availability on a panel due to obstructions but not the localised wind speed and temperature. For this reason, we cannot apply the previously-described preference model to weather scenarios. That is, the meso-climatic variations (and the uncertainty about those variations) apply equally to all urban locations belonging to the same micro-climate. However, decision-makers might be interested in avoiding the risk of installing solar modules in locations that under-perform with respect to a benchmark.

We propose a method based on two weather scenarios, one with ‘typical’ and one with low radiation availability. Simulation with the ‘low rad’ weather scenario is used to discard locations that fall below a certain threshold and an estimate of the annual yield is then calculated using the typical weather results. Subsequently, the ranking is obtained by sorting the annual yields. Although irradiation thresholds are not unequivocal, we think

that they are a useful instrument to define the suitability of a surface, considering the attitude to the payback time: in general, if we neglect economy-of-scale considerations, the higher the threshold, the shorter the payback time of the solar system will be, as only the top-producing PV modules are retained. In this sense, we should consider the minimum acceptable threshold as well as the attitude towards geometric acceptability proposed by Peronato et al. (2015) as variables, which can be selected by the decision maker depending on their preferences.

3. Implementation

The integration of uncertainty in the evaluation of solar energy potential is part of the larger goal of improving current tools for decision making in this field. As pointed out in section 1.2.1, solar cadastres do not consider the aggregated potential of multiple buildings, and they usually implement a 2D visualisation, even when the datasets on which they are based include 2.5D or 3D information, as in the Swiss federal solar cadastre (SFOE-MétéoSuisse-Swisstopo, 2016).

In order to overcome some of these limitations, we implemented the method presented in section 2 in a comprehensive 3D analysis workflow, including the simulation of energy production/need, a risk-aware evaluation through multiple scenarios, and an adapted visualisation technique.

3.1. Workflow

The results presented in this work are based on a modelling and simulation workflow, built upon previous applications at a smaller scale (Peronato et al., 2016b, 2017b) and based on existing state-of-the-art tools, which will be introduced in the following sections. The simulation workflow gives as output a prediction of hourly DC energy production from BIPV modules. These outputs are used as input for the evaluation models developed in this paper, which compute a solar score for each spatial aggregation level that can be finally visualised in a 3D-mapping tool. The flowchart in Figure 3 represents the different steps of the workflow.

3.1.1. Modelling

The calculation of hourly energy production requires the following components: 3D geometry of building surfaces and vegetation, radiative properties of surfaces, hourly irradiance and temperature, and a model of the panel itself.

The simulation input data is constructed from standard 3D geo-datasets (3D cadastre, LiDAR point-cloud, Digital Terrain Model) and hourly weather data (dry-bulb temperature, wind speed, diffuse, and beam radiation). The 3D cadastre is a vector representation of all buildings at Level of Detail (LOD) 2, i.e. including the actual shape of the roof, as well as roof overhangs and main superstructures like dormers. The LiDAR point-cloud is part of an airborne laser scanning (ALS) conducted between March and May 2016 and has a resolution of about 30 pts/m². Two Digital Terrain Models (DTMs) are used in this work: a 1-m resolution DTM for reconstructing the terrain and a 25-m resolution DTM for calculating the far-field obstructions.

The terrain is reconstructed from the DTM using a Delaunay triangulation, while the building surfaces are directly obtained from the 3D cadastre. This method is suitable for large-scale urban simulations, as geodata are tiled in small subsets before analysis. Each 250x250-m tile has an additional 50-m buffer zone to account for shading and reflections from surrounding buildings. These characteristics are similar to the optimal ones (300-m side with 100-m overlap) found by Romero Rodríguez et al. (2017) for a case study in Ludwigsburg in Germany, providing an uncertainty less than 1%. Far-field obstructions like mountains are calculated from a viewpoint at the centre of each tile, 3 m above the ground level, using ArcMap[©] skyline tool. Vegetation is segmented and reconstructed from the LiDAR dataset with a method adapted from Peronato et al. (2016b). However, unlike in Peronato et al. (2016b) which used voxelisation and convex hull algorithms, in this work we implemented an algorithm based on alpha-shape both for segmenting and reconstructing the 3D-shape of the vegetation canopy, also using as input LiDAR points classified as high vegetation (LiDAR class = 5). Alpha-shape algorithms give more realistic tree shapes and have already been used for such applications (Parkan and Tuia, 2018). We used the MATLAB[©] implementation of the algorithm (i.e the function *alphaShape*), with parameters radius = 1.5, HoleThreshold = 10, RegionThreshold = 5, using the facilities provided by the Digital Forestry Toolbox (Parkan, 2017).

We divided the building surfaces (both roofs and façades) into a structured grid (*grid1*) with a fixed distance between the sensor nodes on which the hourly solar irradiances are simulated. A spacing of 2 m (4 m²) was considered a good trade-off between calculation time and accuracy. The discretisation algorithm adds a single sensor point at the centre of those surfaces left without any sensor points at the given resolution. An additional sensor grid (*grid2*) is calculated using the size of a given PV module to consider the effective number of installable modules fitting the building surfaces, and this second grid is used to remap the sensors, as explained in Section 3.1.2.

We used weather data recorded and calculated/modelled at a weather station located in the city of Neuchâtel, Switzerland (NEU). The ‘typical’ weather files used were created from the software Meteonorm (Remund et al., 2012), based on the newest dataset for solar radiation (2000s). The ‘extreme’ weather files were created using measured data for the period 1981-2017. The measured data, i.e. Global Horizontal Irradiation (GHI), Air Temperature and Wind Speed, was downloaded from the Swiss Federal Office of Meteorology and Climatology (MeteoSwiss, 2014), which ensures the quality and availability of weather data for Switzerland. Direct Normal Irradiation (DNI) and Diffuse Horizontal Irradiation (DHI) were modelled from GHI using the model by Reindl et al. (1990) as implemented in Daysim (Reinhart and Herkel, 2000) subprogram *gen_reindl*.

The distribution of GHI over each month in the dataset can be seen in Figure 4 (the box-plots). The difference between annual cumulative GHI for ‘low rad’ and the q10-th quantile year (1992) is +0.5%. The difference between ‘high rad’ and the q90-th quantile year (2009) is -0.1%. These ‘extreme’ weather files are only used here to demonstrate the ranking procedure described in this paper; the point is to illustrate that using only a single typical or average file is unlikely to lead to a robust decision. We encourage the reader to use files suited to their assessment conditions to generate distributions of outcomes.

3.1.2. Simulation

The hourly irradiance (including direct, diffuse and reflected components) is calculated in Daysim (Reinhart and Herkel, 2000). This tool, based on the backwards raytracer Radiance (Ward, 1994), has already been used for assessing the PV potential of roofs (Jakubiec and Reinhart, 2014). Daysim default code was modified to include the horizon obstructions at 10° azimuth resolution.

3D surfaces are assigned short-wave reflective properties, differentiating between ground (reflectance=10%), façades (reflectance=30%), roofs (reflectance=20%), and vegetation (reflectance=20%), considering all of them as Lambertian diffusers. Inter-reflections are included in the simulation, with a maximum limit of two bounces ($-ab = 3$ in Radiance) for backwards ray-tracing from the sensor points to the light source (i.e., the sky patch).

The hourly irradiance values of each PV module (*grid2*) are interpolated from the three closest sensor points with similar normals, simulated on the original *grid1* (2x2-m structured grid), using an inverse distance weighting (IDW) algorithm.

The resulting hourly irradiance values of *grid2* are converted to DC power using the five-parameter model (De Soto et al., 2006) included in the PVLIB toolbox (Holmgren et al., 2015; Holmgren and Groenendyk, 2016). In this application, we considered a commercial mono-crystalline BIPV module.

3.1.3. Evaluation

The evaluation is based on the preference model presented in section 2.3. We consider hence only the uncertainty related to vegetation, while it is possible to run the evaluation selecting only modules above a given production threshold, using the low-yield avoidance method.

The evaluation is carried out using two extreme modelling scenarios, two for each source of uncertainty. The vegetation scenarios require two separate simulations, as new ray-tracing is needed after a change in geometry. Differently, for weather simulation, only the Daysim subprogram *ds_illum* has to be run with a different weather file.

The results are processed in Python scripts to compute the ranking and solar score by using the algorithm presented in section 2.3.1. This algorithm is run at each analysis scale, resulting in a different ranking for each resolution. The results, with the normalised solar score being mapped to a colour-scale, are finally exported as KML files (OGC, 2015), which can be visualised in most 3D-mapping tools.

3.1.4. Visualisation

The results of the evaluation process are visualised in a 3D-mapping tool, based on multiple layers of geo-referenced datasets. The interactive 3D map indicates the priority level of energy refurbishments and/or PV installations in buildings at different spatial aggregation scales.

Each layer represents in fact a spatial aggregation level for which the ranking has been computed. The user can hide or show the layers, in order to have a multi-scale evaluation, or focus on a single layer at a time. The priority level is displayed on false-colour overlays

at the different spatial-aggregation scales, showing the variability of the priority level across the aggregated results (5).

All indicators have the same colour-scale, indicating the normalised score. Despite the possible use of different indicators and normalisation factors, the colour scale is homogeneous across the different analyses and always normalised to the best and worst cases for that location.

3.2. Applicability

The analysis workflow can be applied to any location in which the input data are available. These include notably 3D vector cadastres, LiDAR aerial surveys and historical weather data. In principle, the evaluation can be carried out also on data produced with other 3D-modelling and simulation methods, as long as multiple modelling scenarios can be produced.

Spatial aggregation levels, such as building zones, should also be provided. The relevance of the analysis is in fact dependent on the quality of the spatial aggregation. We should consider homogeneous building zones, which aggregate, for example, all buildings with the same building owner, need for renovation or applicable by-laws.

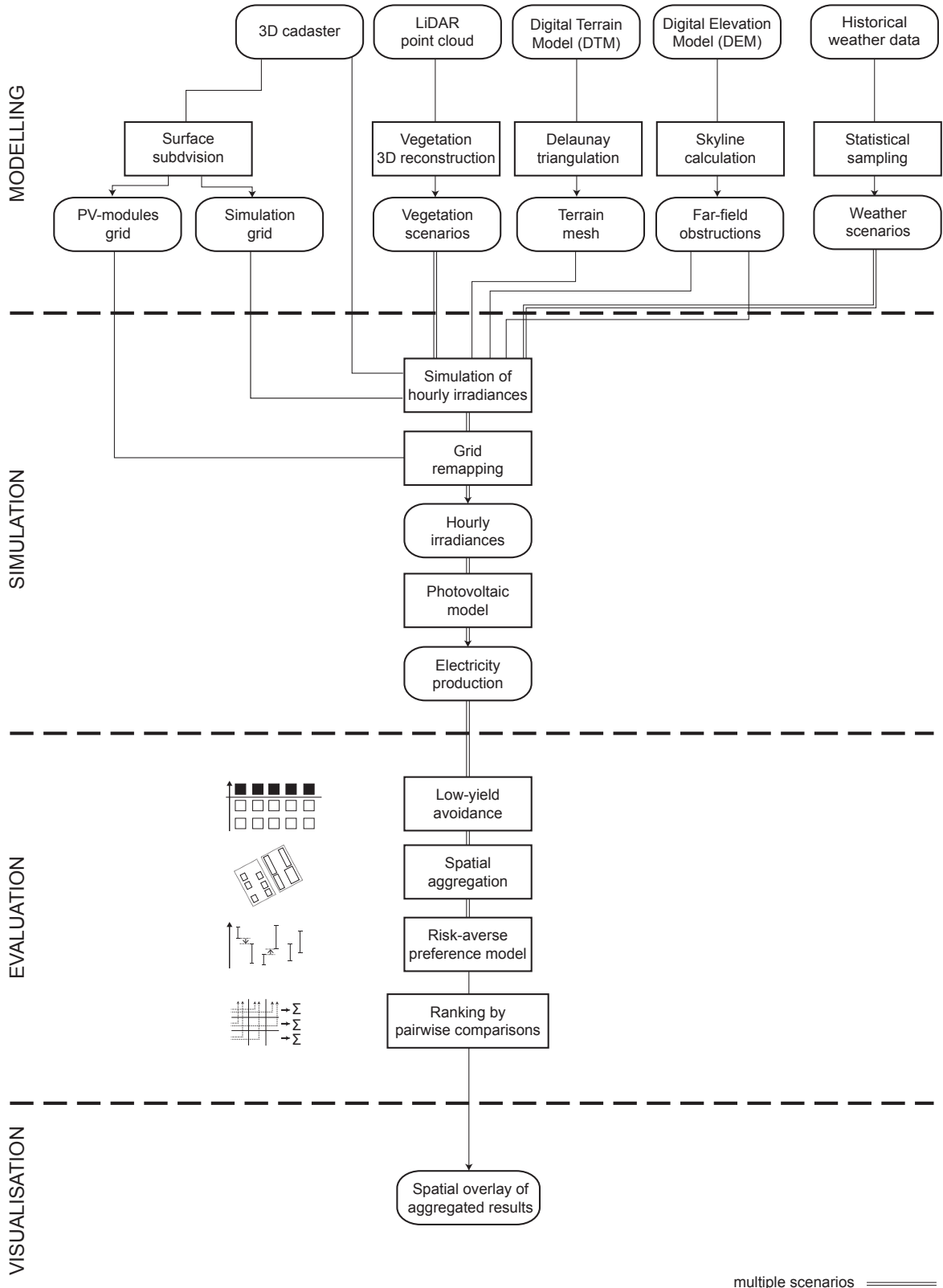


Figure 3: A flowchart representing the different steps of the workflow.
16

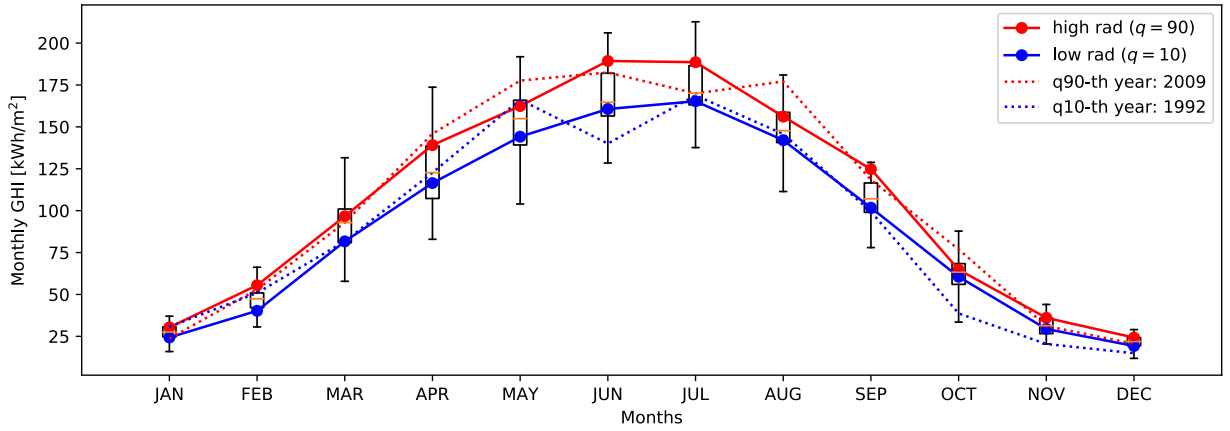


Figure 4: The box-plots show the monthly GHI of MeteoSwiss weather station NEU, located in the city of Neuchâtel, Switzerland, for the period 1981-2017. The box extends from the 25th to 75th quantile of the data, with a line at the median, and the whiskers from the min to the max values. The dotted lines show recorded data for 2009 and 1992, the solid lines ‘extreme’ weather scenarios, whose creation is described in Section 2.2.2. The ‘low rad’ file is composed of concatenated months - from January to December - from the years 1987, 1982, 1992, 2016, 1986, 1999, 1996, 1994, 1988, 1991, 2012, 1986, while the ‘high rad’ file from the years 2007, 2005, 1989, 2014, 2014, 2005, 1985, 1998, 2014, 1986, 1990. Although trend of ‘extreme’ weather scenarios is smoother and the monthly value is in some cases significantly different than the recorded one, the annual GHI of ‘low rad’ (respectively ‘high rad’) is equivalent to the one of the 10-th quantile year 1992 (respectively 90-th quantile year 2009).

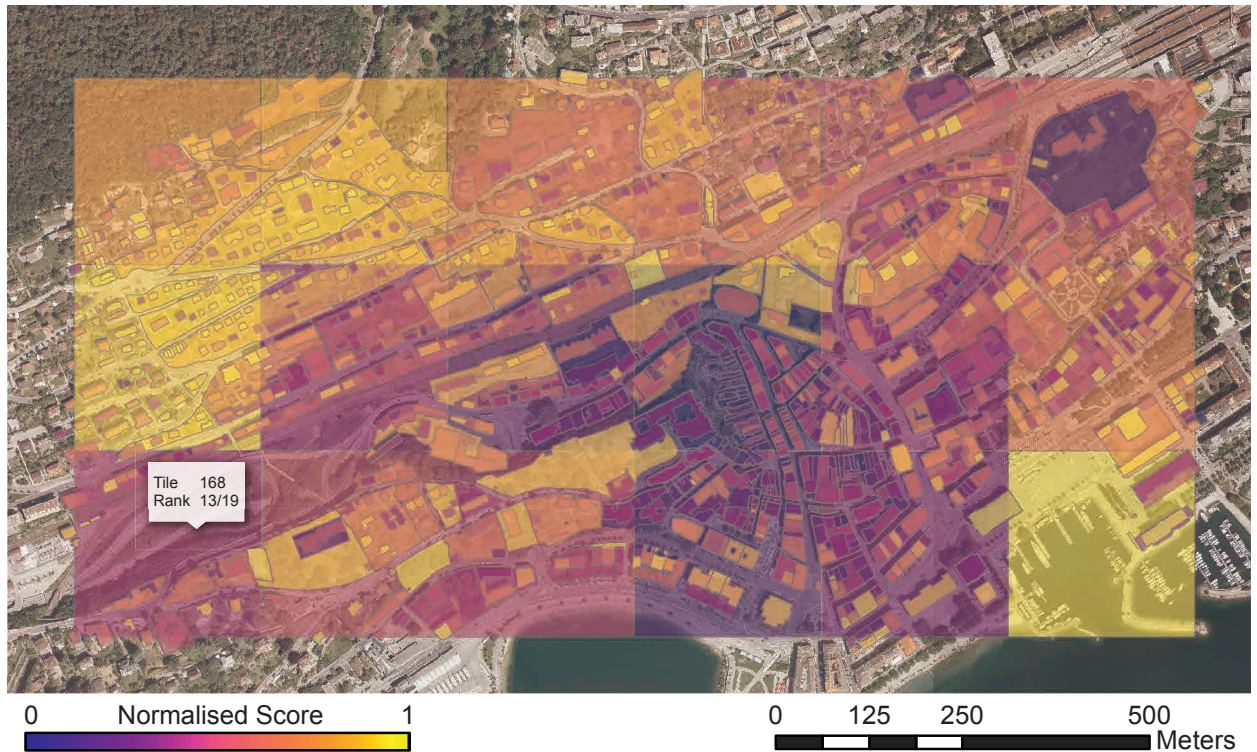


Figure 5: A 2D overlay of three different analysis scales (tile, zone and building) highlights the potential differences within apparently-homogeneous areas (see digital version for colour) with a sample information call-out for tile 168. The colour corresponds to the normalised score of solar potential. By loading the KML files in a 3D-mapping tool, 3D views and interactive consultation of numerical values by clicking on geometry is also possible. Tile 101 is outside this area, so not shown in this picture to maintain the scale. Background orthophoto: ©2016 SITN / Service de la Géomatique et du Registre Foncier.

4. Test application

We now present a test application of our method to a case study in the city of Neuchâtel, Switzerland. We analysed about 1.2 km^2 of dense urban area, encompassing about 1450 buildings.

The analysis was conducted at different spatial resolutions but, for the sake of simplicity and clarity, we present a single spatial resolution only: a ‘tile’. The tile was chosen to present the main results since it limits the number of locations to a manageable number for plotting and discussion while preserving an interesting variability between each location. Similarly, we will limit the analysis to just one metric, which is the gross electric energy production normalised by the peak power installed [kWh/kWp].

4.1. Evaluation

We show here different methods to produce rankings of spatial locations. These rankings, that can be then used to prioritise their building energy retrofit, present a different risk attitude with regards to the considered sources of uncertainty (i.e. vegetation and weather).

4.1.1. Ranking based on single scenarios

As a baseline for comparison, we present the results obtained by ranking tiles based on simulation using a single scenario at a time, i.e., one combination of vegetation and weather. This is the state-of-the-art, i.e., decision-making without consideration of uncertainty. Two sets of results are presented in Figure 6 and Figure 7: tile rankings and scores. The lines have been plotted to show changes between scenarios, so many crossing lines indicate more changes in rankings. The straight lines should not be interpreted to mean that the interpolation between the two extremes is linear. In fact, we do not know the intermediate states since we have not simulated them in this study.

In Figure 6 we can see the ranking based on two vegetation scenarios and a typical weather file. Note that the two vegetation scenarios separately produce two very different rankings. On the contrary, there is very little difference in rankings based on different weather scenarios (simulated without vegetation), as shown in Figure 7.

4.1.2. Ranking based on extreme scenarios

We first analysed the results treating the uncertainty in the factors one-at-a-time, presented in Figure 8. In Figure 8c we can see that median difference in production between weather scenarios is about 0.19 times the ‘high rad’ simulation (19%), while for vegetation, it is about 0.07 times the ‘notrees’ simulation (7%). In other words, for weather scenarios, the magnitude of difference is high, while the spread of variation between tiles is almost null. This means that, while the production values are sensitive to weather, variation in the weather affects all tiles similarly. Conversely, the results for vegetation scenarios show that the magnitude of impact is lower but variation is higher. The vegetation scenarios of individual tiles are varied, but the difference between the extremes is smaller.

When we apply the risk-averse ranking based on pairwise comparison (Section 2.3) to vegetation scenarios under typical weather, with both boolean and fuzzy approaches, the

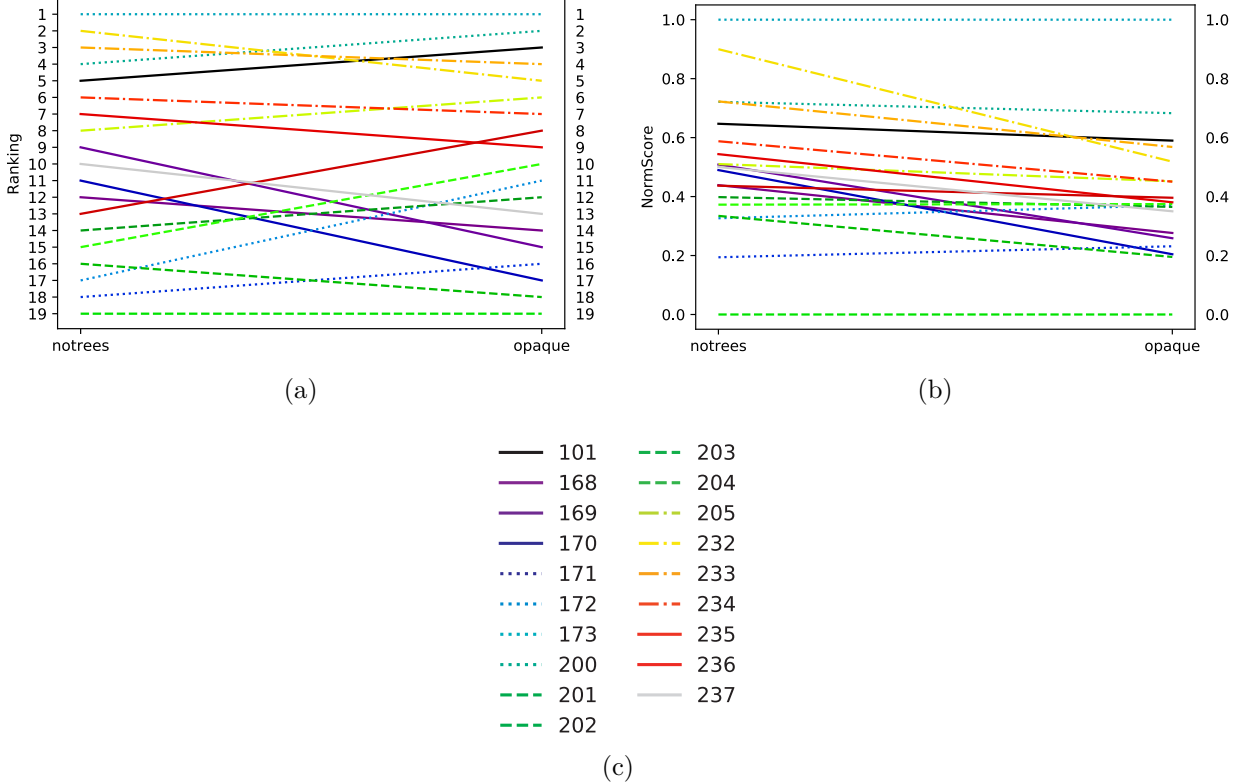


Figure 6: Ranking using single vegetation scenarios: the x-axes represent a scenario while the y-axes represent either rankings (a) or normalised score (b). The ranking (a) is calculated by sorting the gross electric energy production normalised by peak power installed and the score (b) is obtained by a min-max normalization. A large number of crossing lines indicates frequent and significant changes in ranking and scores between the two scenarios, when not considering intermediate ones. The legend (c) shows the tile IDs and the corresponding line style and colour.

decision matrices are visibly different (Figure 9). In the fuzzy approach, only tile 173 and tile 203 clearly stand out respectively for their definite wins and losses, while the other tiles present more subtle differences in the pairwise comparisons.

The results of the ranking aggregation are shown in Figure 10. The overall score is calculated by summing the scores of each line of Figure 9, normalised to a [0, 1] scale (as described in Section 2.3.2). Only 14 out of 19 possible ranks are assigned due to ties. Both the four worst and two best locations have the same rank regardless of the approach. When considering the normalised score, the results have a larger spread than when using the boolean approach. In addition, we see the clusters from the fuzzy evaluation. Converting the normalised scores to rankings causes a loss of information, since small differences between scenarios could produce the same ranks as large differences, provided the sign does not change. This is why we recommend using the normalised score as the best indicator of solar potential, a spatial representation of which is shown in Figure 11. In this map we can see that suburban locations (e.g., tile 200, 232, 233) have higher potential, despite the larger

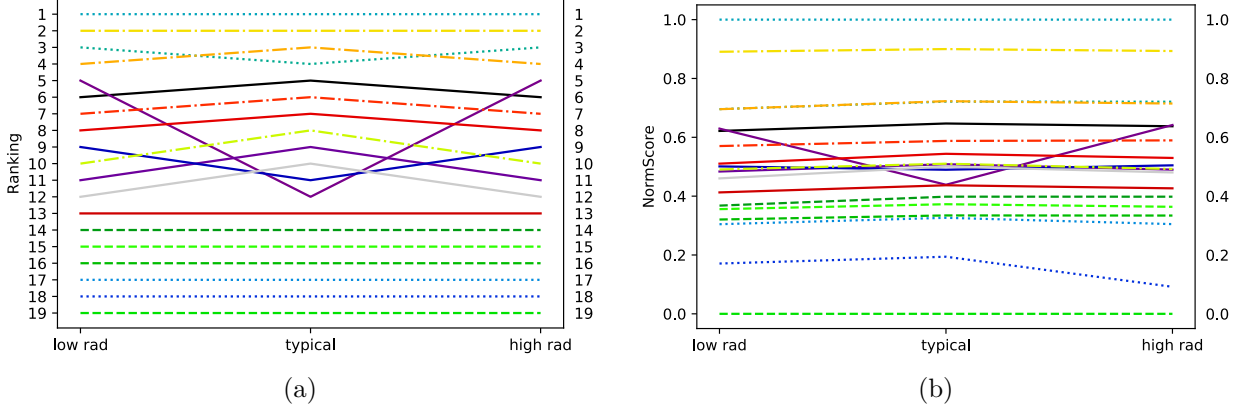


Figure 7: Ranking using single weather scenarios (and ‘notrees’ vegetation conditions): the x-axes represent a weather scenario while the y-axes represent either rankings (a) or score (b). The ranking (a) is calculated by sorting the gross electric energy production normalised by peak power installed and the score (b) is obtained by a min-max normalization. The relatively few changes in the ranking show that the ranking is not very sensitive to the different weather scenarios. The legend in Figure 6c shows the tile IDs and the corresponding line style and colour.

difference between the two vegetation scenarios (Figure 8a).

4.1.3. Low-yield avoidance at different thresholds

As we have seen in the previous section, the absolute difference between production in the radiation scenarios is considerable (in most cases the ‘high rad’ figure is about 1.4 times that of the ‘low rad’ one). While it is intuitive that the production should be very sensitive to solar availability, the decision-maker should consider the magnitude of this variability in the weather of their location. However, as seen in Section 4.1.1, the ranking does not significantly change because of weather. This is in line with our assumption that the mesoclimate and microclimatic variations in solar availability affect all tiles more or less equally.

In order to overcome these limitations as well as those already discussed for the naive ranking (Section 4.1.1), we coupled a simple ranking based on summary statistics with the low-yield-avoidance method. This method excludes those PV modules that do not achieve a given production threshold for a specific weather scenario. Figure 12 shows the ranking considering minimum thresholds t expressed in kWh of module gross electricity production and computed either on the typical weather (‘typical’) or on ‘low rad’ weather scenario (‘conservative’), as well as the naive ranking (already presented in Section 4.1.1 and Figure 6) without threshold ($t = 0$). The ranking and the score are highly affected by the introduction of minimum threshold and, to a minor extent, by the application of the ‘conservative’ weather scenario in the selection of modules.

The ‘conservative’ approach applied to normalised results determines higher potential for all tiles. This is because only the best-performing modules are considered. However, if we consider the non-normalised gross production of a tile shown in Table 1, we see a reduction due to the application of a threshold calculated on a ‘low rad’ weather scenario, especially

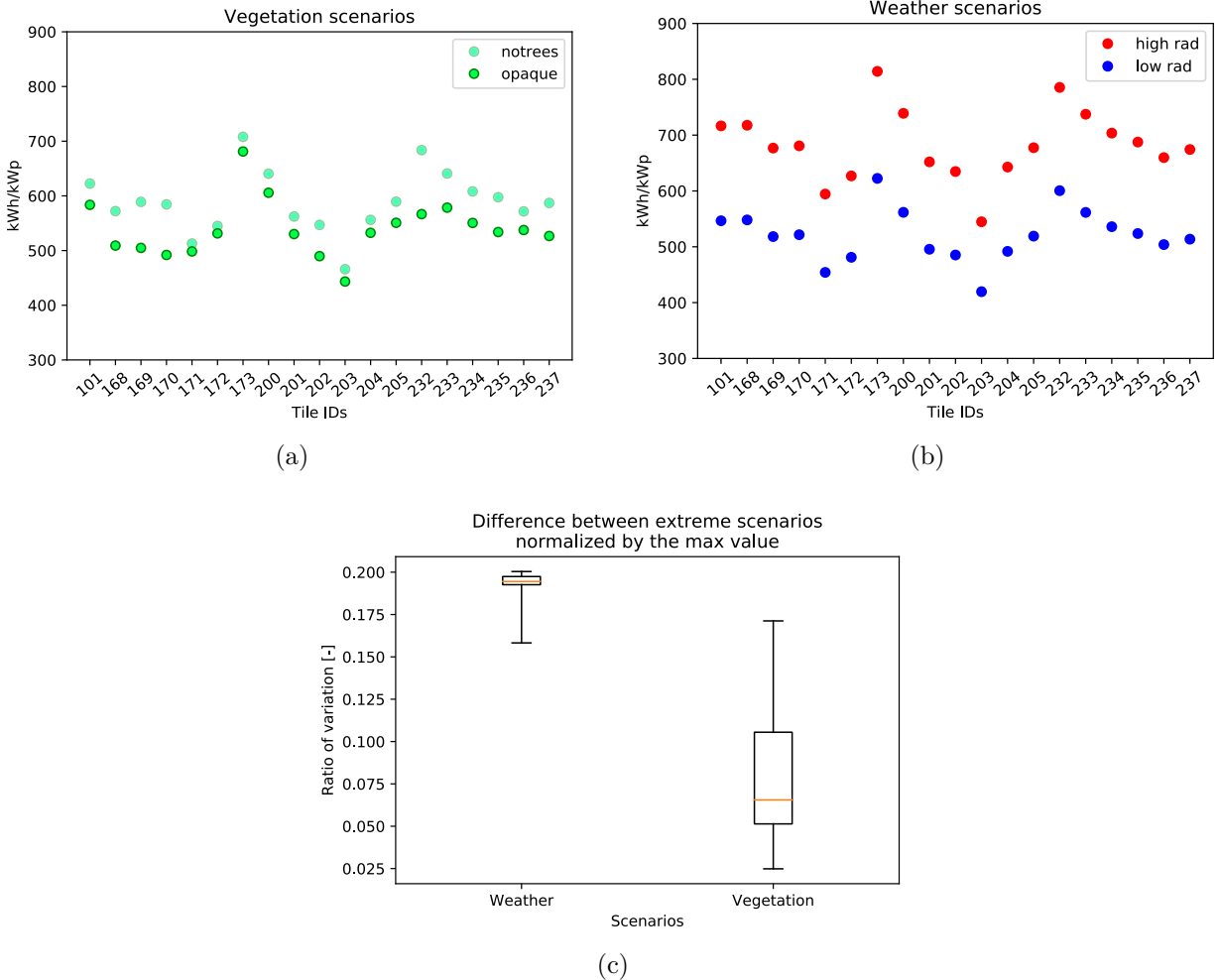


Figure 8: The tile-by-tile scatter plots (a, b) and combined boxplots (c) show the difference of solar potential indicator between the scenarios among the different tiles. In a and b tiles are along the x-axes and the normalised production values are along the y-axes. In a, vegetation scenarios with typical weather are shown. In b, weather scenarios with ‘notrees’ vegetation conditions are shown. The box-plot (c) y-axis is the fractional change from the higher value of production for each tile and the x-axis shows the two considered uncertainty factors (weather and vegetation).

at the upper thresholds. For example, if we discard PV modules not reaching the threshold of 150 kWh yearly production, only about 80% of the production at the ‘typical’ scenario (i.e. using a typical weather file) can be obtained in a ‘conservative’ scenario (i.e. using a ‘low rad’ weather file)

4.2. Random input

We produced randomly-sampled DC production from the vegetation scenarios with the method described in Figure 2. We show the results of 450 vegetation scenarios: 50 randomly-sampled combinations for 9 different increasing ratios of ‘notrees’ and ‘opaque’ scenarios

Table 1: Ratio between non-normalised module gross electricity production calculated using ‘conservative’ and ‘normal’ scenarios at different thresholds. At $t = 0$ the same number of modules are selected for both scenarios, that is why the ratio is 1.

Tile ID	0 kWh	50 kWh	100 kWh	150 kWh	200 kWh
101	1.0	0.99	0.95	0.80	0.92
168	1.0	1.00	1.00	1.07	0.98
169	1.0	0.99	0.96	0.80	0.93
170	1.0	1.00	0.96	0.86	0.87
171	1.0	0.99	0.96	0.91	0.85
172	1.0	0.99	0.97	0.87	0.88
173	1.0	0.99	0.98	0.76	0.90
200	1.0	0.99	0.97	0.73	0.94
201	1.0	0.99	0.97	0.75	0.93
202	1.0	0.99	0.97	0.76	0.91
203	1.0	0.99	0.97	0.92	0.88
204	1.0	0.99	0.97	0.87	0.91
205	1.0	0.99	0.97	0.80	0.93
232	1.0	1.00	0.96	0.87	0.96
233	1.0	0.99	0.95	0.76	0.92
234	1.0	0.99	0.95	0.79	0.91
235	1.0	0.99	0.95	0.79	0.84
236	1.0	0.99	0.96	0.78	0.93
237	1.0	0.99	0.97	0.72	0.91
Average	1.0	0.99	0.97	0.82	0.91

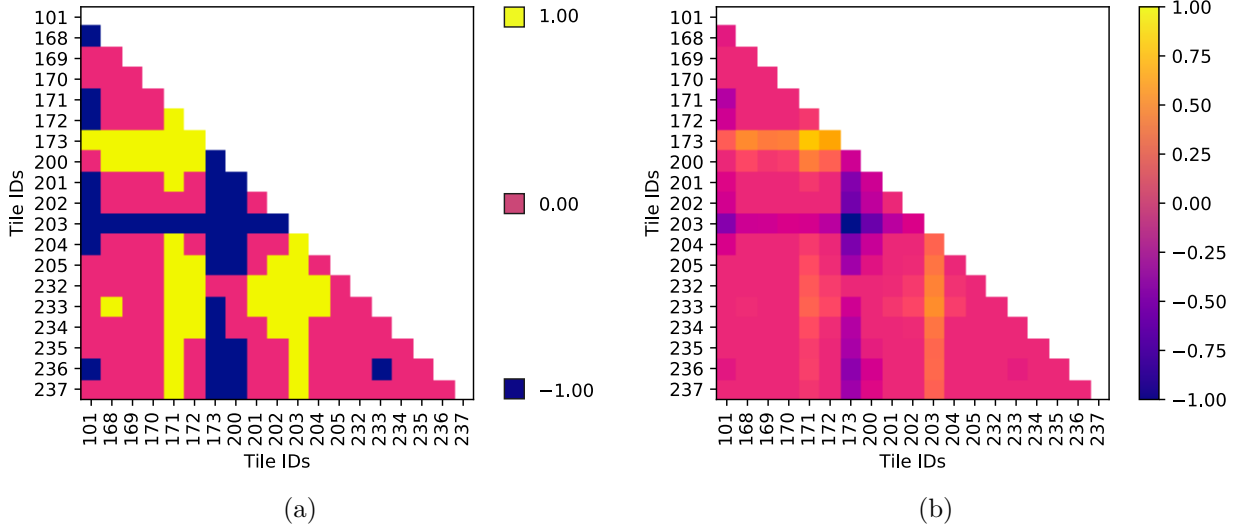


Figure 9: These matrices show the result of risk-averse pairwise comparisons (see Section 2.3) between the different tiles using a boolean (a) or fuzzy (b) logic. The colours represent the score value, as indicated in the colour bar. Each matrix is symmetric along the principal diagonal. Only the lower triangle is shown here; the upper triangle will have the same values with opposite signs.

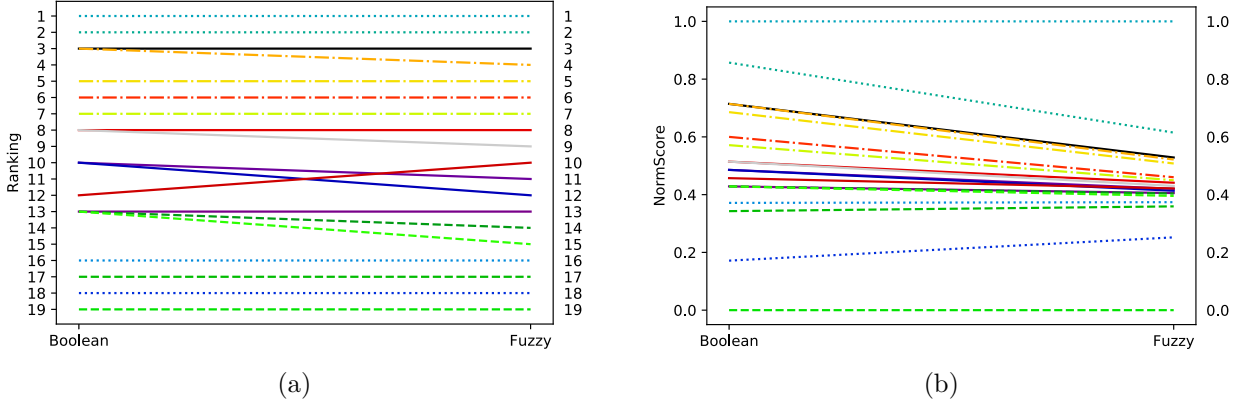


Figure 10: Ranking vegetation scenarios from risk-averse pairwise comparisons (see Section 2.3): a) shows the ranking and b) the normalised score. The fuzzy evaluation helps identify some clusters of tiles with similar scores (e.g. there is a large number of tiles with a score of about 0.45). The legend in Figure 6c shows the tile IDs and the corresponding line style and colour.

(from 0.1 to 0.9). The ratios are a proxy for partial-obstruction, as if each tree was either completely obstructing a panel at some time or not.

Figure 13 shows that the randomly-sampled data does not provide any additional information compared to the extreme scenarios of Figure 8b. In fact the box plots are symmetrical with respect to the median, i.e., the first and third quartiles are always positioned at the same distance from the extremes. This implies that the distribution of the output is completely governed by the sampling distribution of ratios. Testing with other distributions

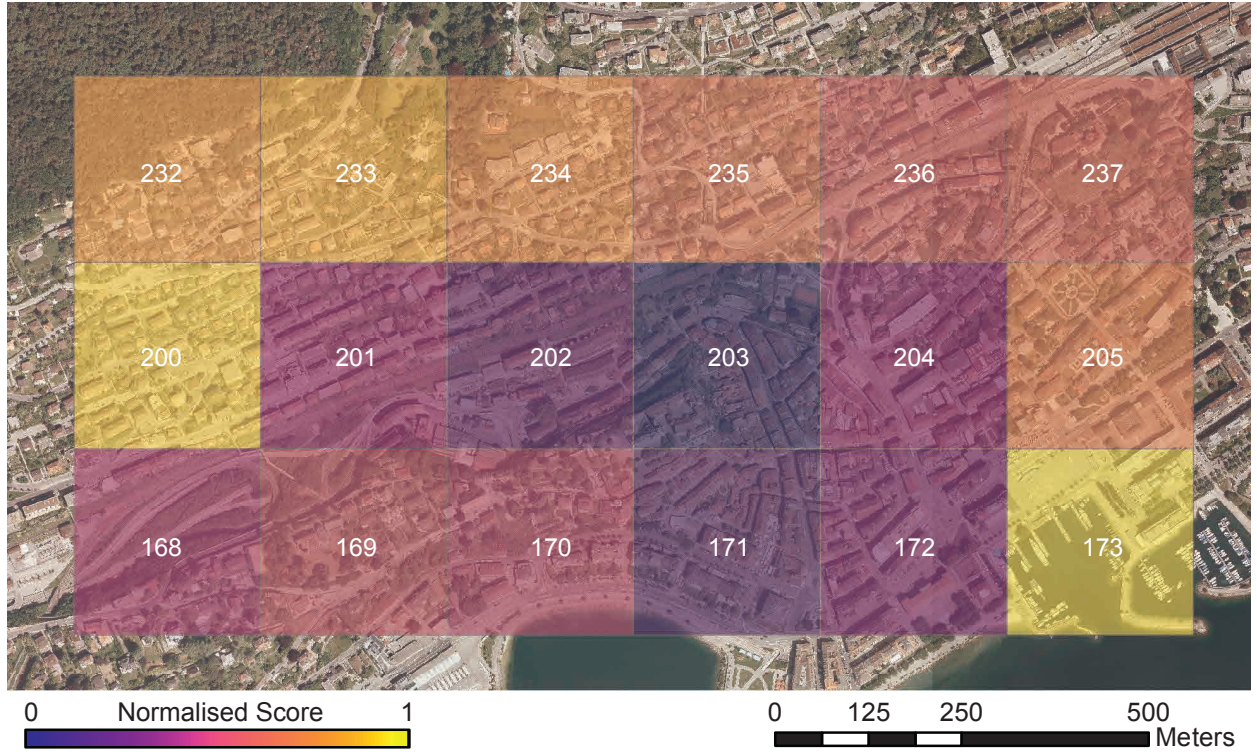


Figure 11: Results of vegetation analysis using a fuzzy approach: normalised score displayed as false colours shows that the best tiles are in the lower-density areas. The tile ID is shown at the centre of each tile. Tile 101 is outside this area, so not shown in this picture to maintain the scale. Background orthophoto: ©2016 SITN / Service de la Géomatique et du Registre Foncier.

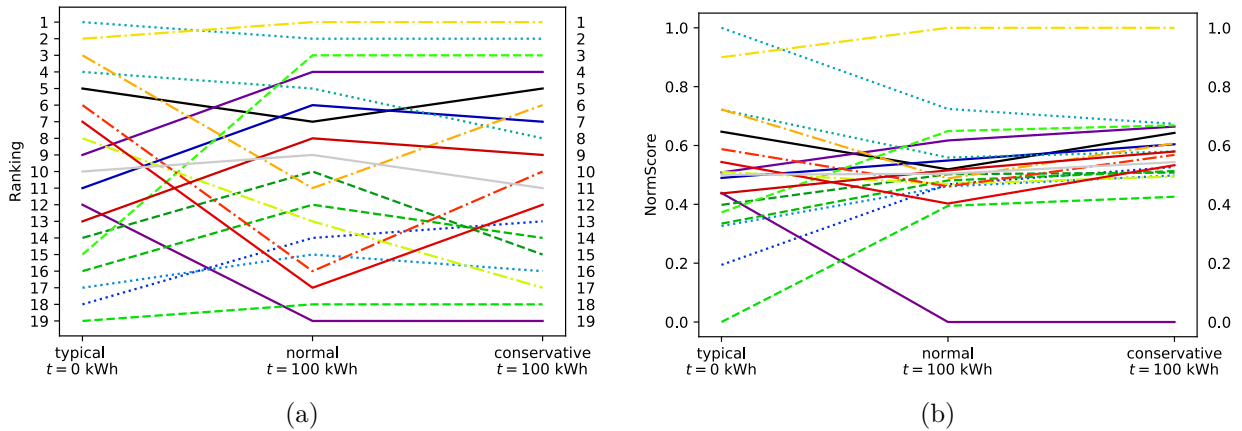


Figure 12: Ranking with a threshold applied on typical weather file ('typical') or 'low rad' weather scenario ('conservative'): a)) shows the ranking and b) the normalised score. The numerous crossing lines show that the use of thresholds, as well as of a 'conservative' risk-attitude, have a high impact on ranking and score. The legend in Figure 6c shows the tile IDs and the corresponding line style and colour.

confirmed this. The reason for this and potential improvements to the random sampling are discussed in Section 5.

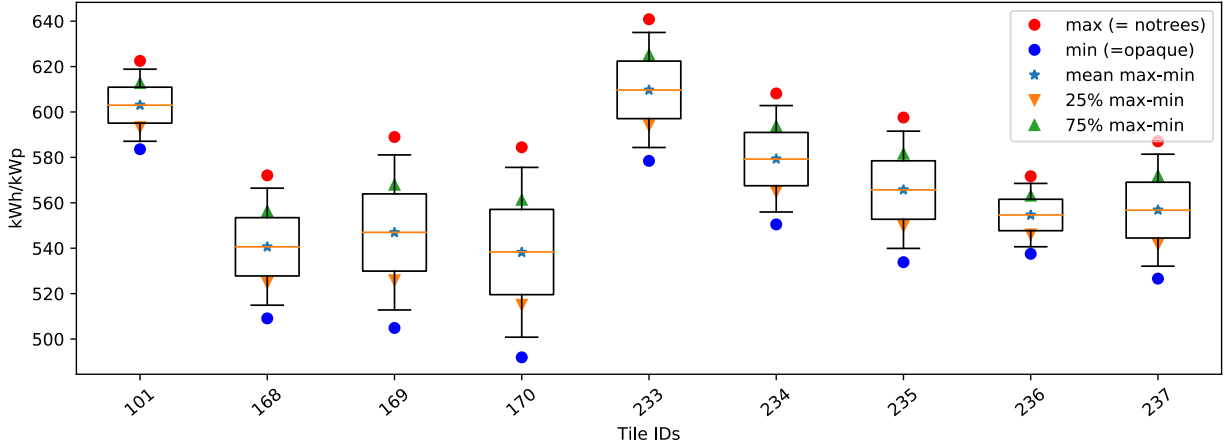


Figure 13: Boxplot of simulation outputs from randomly-sampled vegetation scenarios (only a subset of tiles is shown here). The ratios of obstructed:unobstructed sensors were sampled as described in Figure 2, i.e., from a uniform distribution.

4.3. Summary of findings

The application to the case-study of Neuchâtel highlighted the potential of the proposed method. We summarise here the main lessons learnt: first, the ones related to the case-specific application in Neuchâtel, and, second, those that we assume can be generalised also to other applications.

4.3.1. Case-specific findings

We have seen that, despite the high influence of vegetation in the absolute results, suburban tiles rank better for solar potential compared to the ones located in the dense historical city centre. By using a fuzzy approach, it was possible to establish an unique rank (i.e. without any tie) for every tile, which could be used to assign limited resources for building energy retrofit by prioritizing those with a greater potential. The best- and worst-classified tiles were stable among the different rankings, except when minimum thresholds were applied. In this sense, if we exclude PV modules on façades, which are more likely affected by the surrounding obstructions, by imposing a minimum threshold, also buildings in central areas present an interesting potential.

However, we should consider that the tile level, which was shown here only for sake of brevity, does not correspond to an adequate spatial aggregation criteria. For example, in this sample application, tile 173 always outranks its competitors due to the low number of buildings, which are well exposed. The application to homogeneous building zones or single buildings should be therefore preferred.

4.3.2. General findings

The case-study application showed that both the ranking and the absolute production values of spatial locations are highly influenced by the choice of the modelling scenario.

In the case of vegetation, i.e. a typical epistemic uncertainty related to the difficulties of remote-sensing and modelling reality, the ranking is significantly changing depending on the considered modelling scenario, although the absolute difference between the scenarios is relatively small. The opposite happens for weather uncertainty, which is temporally aleatory but spatially constant, as the proposed method does not consider local variations inside the same urban area.

We can conclude that weather uncertainty has an impact in sorting problems (as some locations could fall below the threshold), but does not influence a ranking problem such as the one of prioritizing locations.

5. Discussion

The proposed method is an alternative to existing evaluations methods of building solar potential, such as solar scores and threshold-based sorting of building surfaces, and is complementary to works considering heritage protection (López and Frontini, 2014) and visibility (Florio et al., 2016). The goal is not to define the actual yield of the solar panels during their life-time but to establish a ranking of the most suitable locations and avoid those that risk underperforming. Unlike solar cadastres, which are typically targeted only at building owners, our method integrates different spatial aggregation scales. Although we show here an application with a single indicator of solar potential (gross electricity production normalised by the peak power installed), the method can be extended to other metrics, including for example an estimation of building electricity consumption, as well as other normalization factors, such as the building floor area or footprint area.

As far as limitations go, we only analysed weather- and vegetation-related uncertainty. However, there are other uncertain inputs that might influence the results and should be considered to obtain a more robust evaluation of the solar potential. For example, we have not considered the uncertainty related to the visual acceptability of the proposed installation. As shown by Peronato et al. (2015), the attitude of the decision-maker with regards to the geometric regularity of the arrangement of solar modules might influence the results depending on the threshold. Like vegetation, these attitudes can be summarised by two extreme scenarios – aggressive or conservative – and integrated into the decision process.

We also assumed that there is no interaction between the physical properties of a panel and the uncertain boundary conditions. This assumption is a simplification, and may not hold true if the decision-maker is considering different panel types and installations, whose response to the incident solar radiation and ambient temperature is not constant. For example, amorphous and mono-crystalline panels respond differently to direct and diffuse radiation, so the prevalence of one or the other will result in different patterns of electric production under the same environmental conditions. If the decision-maker is interested in comparing different panel types for different plots, then presumably the virtual models of each panel-plot combination should reflect these differing physical properties and responses

in the production simulation. That is, a plot can be thought of as having variants, e.g., plot 1 with amorphous, plot 1 with mono-crystalline, plot 2 with amorphous, plot 2 with mono-crystalline, and so on.

We further assumed that the interaction between weather and obstruction is unknown, *a priori*. If the vegetation blocks the solar access of a sensor point consistently throughout a year, comparing a single value of the summary statistic might result in a very similar ranking to comparing distributions of summary statistics. If, however, the vegetation tends to block the sun inconsistently, or a climate shows strong seasonal variation in cloud cover, then the amount of production from a single panel could show high variance. The upshot is that these results can not be estimated without actually doing the comparisons with uncertain inputs.

In terms of analysis workflow, the main limitations are related to the availability of the 3D geodata, in particular of vector 3D cadastres which are used for the simulation of the solar irradiation. Moreover, despite the accuracy of this 3D geometry, windows and balconies are not present in the model and for this reasons only simplifying assumptions can be done on the effective possibility of façade-mounted PV modules.

6. Conclusion

In this work, we presented a decision-support toolkit to prioritise spatial locations based on their solar energy potential. Unlike current solar cadastres, which have a deterministic approach towards solar potential associating each spatial location with a given energy production, we incorporated uncertainty through a ranking-based evaluation of spatial locations. The proposed risk-averse ranking method helps consider input uncertainty in a systematic manner that can be used to allocate limited resources.

In order to test the proposed methodology, we have considered vegetation modelling and weather as the two possible source of uncertainty and tested it in a case study comprising about 1450 buildings. We have seen that the ranking of the different changes is highly impacted by the vegetation modelling scenario, highlighting the importance of integrating vegetation-related uncertainty in a decision-support method. On the other hand, despite the large absolute difference in the results between the considered weather scenarios, the ranking is not affected by the use of these scenarios. Unlike the findings of Rastogi (2016) for building energy performance, in our work we have found a linear response of photovoltaic energy production to weather scenarios and no interaction with vegetation. Nonetheless, we showed that the ranking changes if we remove low-production panels based on a threshold, minimising the risk of non-optimal panel location.

Modelling extreme scenarios is a simple and effective method when decision-makers are risk-averse, which is likely the case in the public sector. In addition to using extreme scenarios to define variability intervals for the input data, we have seen that these can also be used as input for random sampling. We have constructed the framework for incorporating sampling of uncertain inputs for decision-making. Future work could include the collection of data to provide informative prior distributions and perhaps provide a wider range of risk-taking attitudes to decision-makers, as Monte-Carlo estimates of summary statistics could

be different from comparisons using the extreme scenarios only.

The proposed method allows a relative comparison of solar power installations at many spatial locations through the calculation of a solar score. Incorporated this in a mapping tool allows the user to interact and visualise the results through false-colour semi-transparent overlays on a map and consultation pop-ups (Figure 5), highlighting internal differences within the same plot such as, for example, a high-potential building in a low-potential area. We see its possible application as an urban planning tool targeted at both public authorities and large private or public real estate owners, while its effectiveness and value should be proved by test applications with these stakeholders.

We argue that the inclusion of some sources of uncertainty in the calculation of such a score gives a more robust evaluation of the solar potential, for use in evidence-based planning decisions, in particular to prioritise different buildings and zones in view of building energy retrofit, and in fairness-sensitive applications, such as public fund allocation.

Acknowledgments

This work has been conducted in the framework of the ACTIVE INTERFACES research project (Rey et al., 2015), which is part of the National Research Programme ‘Energy Turn-around’ (NRP 70) of the Swiss National Science Foundation (SNSF). Further information on the National Research Programme can be found at <http://www.nrp70.ch>.

G.P. and P.R. acknowledge additional financial support respectively from the Ecole polytechnique fédérale de Lausanne (EPFL) and from the Swiss National Science Foundation (SNSF) - Early PostDoc.Mobility fellowship.

The geodata used in this work have been kindly provided by the Système d’Information du Territoire Neuchâtelois - SITN (Digital Terrain Model at 1-m resolution, LiDAR dataset and 3D cadastre) and by the Swiss Federal Office of Topography - Swisstopo (Digital Terrain Model at 25-m resolution)

The authors would like to thank Prof. François Golay for his useful feedback on the decision-making method and Matthew Parkan for the help with the vegetation reconstruction.

References

- Berlin, E., Reinhart, C., Jakubiec, A., Waissbluth, N., 2013. Mapdwell.
URL <http://www.mapdwell.com/en>
- Brans, J., 1982. L’ingénierie de la décision. Elaboration d’instruments d’aide à la décision. Méthode PROMETHEE. Laide à La Decision: Nature, Instrument Set Perspectives Davenir, 183–214.
- Bremer, M., Mayr, A., Wichmann, V., Schmidtner, K., Rutzinger, M., May 2016. A new multi-scale 3d-GIS-approach for the assessment and dissemination of solar income of digital city models. Computers, Environment and Urban Systems 57, 144–154.
URL <http://www.sciencedirect.com/science/article/pii/S0198971516300151>
- Brito, M. C., Freitas, S., Guimaraes, S., Catita, C., Redweik, P., Oct. 2017. The importance of facades for the solar PV potential of a Mediterranean city using LiDAR data. Renewable Energy 111, 85–94.
URL <http://www.sciencedirect.com/science/article/pii/S0960148117302768>

- Catita, C., Redweik, P., Pereira, J., Brito, M. C., May 2014. Extending solar potential analysis in buildings to vertical facades. *Computers & Geosciences* 66, 1–12.
 URL <http://www.sciencedirect.com/science/article/pii/S0098300414000053>
- Cebecauer, T., Suri, M., May 2015. Typical Meteorological Year Data: SolarGIS Approach. *Energy Procedia* 69, 1958–1969.
 URL <http://www.sciencedirect.com/science/article/pii/S1876610215005019>
- De Soto, W., Klein, S. A., Beckman, W. A., Jan. 2006. Improvement and validation of a model for photovoltaic array performance. *Solar Energy* 80 (1), 78–88.
 URL <http://www.sciencedirect.com/science/article/pii/S0038092X05002410>
- Dean, J., Kandt, A., Burman, K., Lisell, L., Helm, C., 2009. Analysis of web-based solar photovoltaic mapping tools. In: ASME 2009 3rd International Conference on Energy Sustainability collocated with the Heat Transfer and InterPACK09 Conferences. American Society of Mechanical Engineers, pp. 85–96.
- Dobos, A. P., Gilman, P., Kasberg, M., 2012. P50/P90 Analysis for Solar Energy Systems Using the System Advisor Model. In: Proceedings of the WREF 2012. National Renewable Energy Laboratory (NREL), Golden, CO.
- Feizizadeh, B., Shadman Roodposhti, M., Jankowski, P., Blaschke, T., Dec. 2014. A GIS-based extended fuzzy multi-criteria evaluation for landslide susceptibility mapping. *Computers & Geosciences* 73 (Supplement C), 208–221.
 URL <http://www.sciencedirect.com/science/article/pii/S0098300414001873>
- Florio, P., Roecker, C., Probst, M. C. M., Scartezzini, J.-L., 2016. Visibility of Building Exposed Surfaces for the Potential Application of Solar Panels: A Photometric Model. The Eurographics Association.
 URL <https://diglib.eg.org:443/handle/10.2312/udmv20161419>
- Freitas, S., Catita, C., Redweik, P., Brito, M. C., Jan. 2015. Modelling solar potential in the urban environment: State-of-the-art review. *Renewable and Sustainable Energy Reviews* 41, 915–931.
 URL <http://www.sciencedirect.com/science/article/pii/S1364032114007461>
- Holmgren, W. F., Andrews, R. W., Lorenzo, A. T., Stein, J. S., Jun. 2015. PVLIB Python 2015. In: 2015 IEEE 42nd Photovoltaic Specialist Conference (PVSC). pp. 1–5.
- Holmgren, W. F., Groenendyk, D. G., Jun. 2016. An open source solar power forecasting tool using PVLIB-Python. In: 2016 IEEE 43rd Photovoltaic Specialists Conference (PVSC). pp. 0972–0975.
- Jakubiec, J., Reinhart, C., Dec. 2014. Assessing Disability Glare Potential of Reflections from New Construction. *Transportation Research Record: Journal of the Transportation Research Board* 2449, 114–122.
 URL <http://trrjournalonline.trb.org/doi/abs/10.3141/2449-13>
- Jakubiec, J. A., Reinhart, C. F., Jul. 2013. A method for predicting city-wide electricity gains from photovoltaic panels based on LiDAR and GIS data combined with hourly Daysim simulations. *Solar Energy* 93, 127–143.
 URL <http://www.sciencedirect.com/science/article/pii/S0038092X13001291>
- Kanters, J., Wall, M., Kjellsson, E., 2014. The Solar Map as a Knowledge Base for Solar Energy Use. *Energy Procedia* 48, 1597–1606.
 URL <http://www.sciencedirect.com/science/article/pii/S1876610214004421>
- Kim, Y., Chung, E.-S., Jun, S.-M., Kim, S. U., Apr. 2013. Prioritizing the best sites for treated wastewater instream use in an urban watershed using fuzzy TOPSIS. *Resources, Conservation and Recycling* 73, 23–32.
 URL <http://www.sciencedirect.com/science/article/pii/S0921344912002236>
- Korpela, I., Ørka, H., Maltamo, M., Tokola, T., Hyppä, J., 2010. Tree species classification using airborne LiDAR – effects of stand and tree parameters, downsizing of training set, intensity normalization, and sensor type. *Silva Fennica* 44 (2).
 URL <http://www.silvafennica.fi/article/156>
- Liang, S., de Alfaró, L., 2017. Efficient Selection of Pairwise Comparisons for Computing Top-heavy Rankings.
- López, C. S. P., Frontini, F., 2014. Energy Efficiency and Renewable Solar Energy Integration in Heritage Historic Buildings. *Energy Procedia* 48, 1493–1502.

- URL <http://www.sciencedirect.com/science/article/pii/S1876610214004317>
- Malczewski, J., 1999. GIS and multicriteria decision analysis. John Wiley & Sons, Inc., New York.
- Malczewski, J., Rinner, C., 2015. Dealing with Uncertainties. In: Multicriteria Decision Analysis in Geographic Information Science. Advances in Geographic Information Science. Springer, Berlin, Heidelberg, pp. 191–221.
- URL https://link.springer.com/chapter/10.1007/978-3-540-74757-4_7
- MeteoSwiss, 2014. IDAWEB.
- URL <https://gate.meteoswiss.ch/idaweb/system/welcome.do>
- Miller, R., Herrmann, D., Apr. 2016. System and method for producing suitability score for energy management system on building rooftop.
- URL <https://www.google.ch/patents/US20160110663>
- Naderi, S. H., Shams, P., Shahhoseini, H. S., Jun. 2012. Fuzzy-Copeland ranking method to evaluate multi-disjoint paths selection algorithms. In: 2012 IEEE International Conference on Computer Science and Automation Engineering. pp. 761–764.
- Nault, E., Peronato, G., Andersen, M., 2015. Forme urbaine et potentiel solaire. In: Rey, E. (Ed.), Urban Recovery. Presses Polytechniques et Universitaires Romandes (PPUR), Lausanne.
- OGC, 2015. OGC KML 2.3.
- Ouhajjou, N., Loibl, W., Anjomshoaa, A., Fenz, S., Tjoa, A. M., Aug. 2014. Ontology-based urban energy planning support building-integrated solar PV. In: eWork and eBusiness in Architecture, Engineering and Construction. CRC Press, pp. 543–550.
- URL <http://www.crcnetbase.com/doi/abs/10.1201/b17396-89>
- Ouhajjou, N., Loibl, W., Fenz, S., Tjoa, A. M., Nov. 2015. Stakeholder-oriented Energy Planning Support in Cities. In: Energy Procedia. Vol. 78. pp. 1841–1846.
- Ouhajjou, N., Loibl, W., Fenz, S., Tjoa, A. M., 2016. Multi-actor Urban Energy Planning Support: Building Refurbishment & Building-Integrated Solar PV. In: Advances and New Trends in Environmental and Energy Informatics. Progress in IS. Springer, Cham, pp. 157–176.
- URL https://link.springer.com/chapter/10.1007/978-3-319-23455-7_9
- Parkan, M., 2017. Digital-Forestry-Toolbox: A Collection of Digital Forestry Tools for Matlab.
- URL <http://mparkan.github.io/Digital-Forestry-Toolbox/>
- Parkan, M., Tuia, D., Feb. 2018. Estimating Uncertainty of Point-Cloud Based Single-Tree Segmentation with Ensemble Based Filtering. Remote Sensing 10 (2), 335.
- URL <http://www.mdpi.com/2072-4292/10/2/335>
- Peronato, G., Bonjour, S., Stoeckli, J., Rey, E., Andersen, M., Jul. 2016a. Sensitivity of calculated solar irradiation to the level of detail: insights from the simulation of four sample buildings in urban areas. In: PLEA 2016 - Cities, Buildings, People: Towards Regenerative Environments, Proceedings of the 32nd International Conference on Passive and Low Energy Architecture;. Vol. 2. Los Angeles.
- Peronato, G., Rastogi, P., Andersen, M., 2017a. Robustesse de l'évaluation du potentiel solaire de formes urbaines différencierées. In: Rey, E. (Ed.), Suburban polarity. Presses Polytechniques et Universitaires Romandes (PPUR), Lausanne.
- Peronato, G., Rey, E., Andersen, M., 2015. Sampling of building surfaces towards an early assessment of BIPV potential in urban contexts. In: Proceedings of PLEA2015 Architecture in (R)Evolution. Bologna.
- URL <http://www.plea2015.it/book/download.php?id=642>
- Peronato, G., Rey, E., Andersen, M., Oct. 2016b. 3d-modeling of vegetation from LiDAR point clouds and assessment of its impact on façade solar irradiation. In: ISPRS - International Archives of the Photogrammetry, Remote Sensing and Spatial Information Sciences. Vol. XLII-2/W2. Athens, pp. 67–70.
- Peronato, G., Rey, E., Andersen, M., 2017b. ACTIVE INTERFACES. From 3d geodata to BIPV yield estimation: towards an urban-scale simulation workflow.
- URL <https://infoscience.epfl.ch/record/226576>
- Pomerol, J.-C., Barba-Romero, S., Dec. 2012. Multicriterion Decision in Management: Principles and Practice. Springer Science & Business Media, google-Books-ID: sk.hBwAAQBAJ.
- Rastogi, P., Aug. 2016. On the sensitivity of buildings to climate: the interaction of weather and building

- envelopes in determining future building energy consumption. PhD, Ecole polytechnique fédérale de Lausanne, Lausanne, Switzerland, doi:10.5075/epfl-thesis-6881.
- URL <https://infoscience.epfl.ch/record/220971?ln=en>
- Reindl, D. T., Beckman, W. A., Duffie, J. A., Jan. 1990. Diffuse fraction correlations. *Solar Energy* 45 (1), 1–7.
- URL <http://www.sciencedirect.com/science/article/pii/0038092X9090060P>
- Reinhart, C. F., Herkel, S., Jul. 2000. The simulation of annual daylight illuminance distributions — a state-of-the-art comparison of six RADIANCE-based methods. *Energy and Buildings* 32 (2), 167–187.
- URL <http://www.sciencedirect.com/science/article/pii/S037877880000426>
- Remund, J., Mueller, S., Kunz, S., Schilter, C., May 2012. METEONORM Handbook Part II : Theory. Tech. rep.
- URL <http://meteonorm.com/download/software/mn70/>
- Rey, E., Lufkin, S., Ballif, C., Wuestenhagen, R., Wittkopf, S., Bacher, J.-P., Apr. 2015. Building integrated photovoltaics | ACTIVE INTERFACES.
- Romero Rodríguez, L., Nouvel, R., Duminil, E., Eicker, U., Nov. 2017. Setting intelligent city tiling strategies for urban shading simulations. *Solar Energy* 157, 880–894.
- URL <http://www.sciencedirect.com/science/article/pii/S0038092X17307855>
- Roy, B., Vincke, P., 1984. Relational Systems of Preference with One or More Pseudo-Criteria: Some New Concepts and Results. *Management Science* 30 (11), 1323–1335.
- URL <http://www.jstor.org/stable/2631567>
- Saaty, T. L., 1980. The Analytic Hierarchy Process: Planning, Priority Setting, Resource Allocation. McGraw-Hill, google-Books-ID: Xxi7AAAAIAAJ.
- Schärlig, A., 1985. Décider sur plusieurs critères: Panorama de l'aide à la décision multicritère. Presses Polytechniques et Universitaires Romandes (PPUR).
- Schärlig, A., 1996. Pratiquer Electre et Prométhée. Presses Polytechniques et Universitaires Romandes (PPUR).
- SFOE-MétéoSuisse-Swisstopo, 2016. Toit solaire. Swiss Federal Office of Energy SFOE - Federal Office of Meteorology and Climatology MeteoSwiss - Federal Office of Topography swisstopo <http://www.uvek-gis.admin.ch/BFE/sonnendach/?lang=en>.
- URL www.toit-solaire.ch
- Shah, N. B., Wainwright, M. J., Dec. 2015. Simple, Robust and Optimal Ranking from Pairwise Comparisons. arXiv:1512.08949 [cs, math, stat]ArXiv: 1512.08949.
- URL <http://arxiv.org/abs/1512.08949>
- Vignola, F., Grover, C., Lemon, N., McMahan, A., Aug. 2012. Building a bankable solar radiation dataset. *Solar Energy* 86 (8), 2218–2229.
- URL <http://www.sciencedirect.com/science/article/pii/S0038092X1200182X>
- Ward, G. J., 1994. The RADIANCE lighting simulation and rendering system. In: Proceedings of the 21st annual conference on Computer graphics and interactive techniques. SIGGRAPH '94. ACM, New York, NY, USA, pp. 459–472.
- Wilcox, S., Marion, W., May 2008. Users' Manual for TMY3 Data Sets. Tech. rep.
- URL <http://www.nrel.gov/docs/fy08osti/43156.pdf>